Bull. Mater. Sci., Vol. 36, No. 5, October 2013, pp. 923–929. © Indian Academy of Sciences.

Electronic spectra of anions intercalated in layered double hydroxides

S RADHA and P VISHNU KAMATH*
Department of Chemistry, Central College, Bangalore University, Bangalore 560 001, India

MS received 14 February 2012; revised 4 September 2012

Abstract. **Transition metal complexes intercalated in layered double hydroxides have a different electronic structure as compared to their free state owing to their confinement within the interlayer gallery. UV–Vis absorptions of the intercalated complex anions show a significant shift as compared to their free state. The ligand to metal charge transfer transitions of the ferricyanide anion show a red shift on intercalation. The ferrocyanide ion shows a significant blue shift of *d–d* bands due to the increased separation between t_{2g} and e_g levels on intercalation. MnO_4^- ion shows a blue shift in its ligand to metal charge transfer transition since the non-bonding t_1 level of oxygen from which the transition arises is stabilized.**

Keywords. **Layered double hydroxides; intercalation; electronic spectroscopy.**

1. Introduction

Layered double hydroxides (LDHs) constitute an important class of inorganic materials which comprise positively charged layers having the composition, $[M^{II}_{1-x}Al_x(OH)_2]^{x+}$ ($x = 0{\cdot}33$, M = Zn in this work), incorporating anions in the interlayer for charge neutrality (Miyata 1975). A typical LDH has the composition, $[Zn_{0{\cdot}67}Al_{0{\cdot}33}(OH)_2](A^{n-})_{0{\cdot}33/n}\cdot yH_2O$ (A = CO_3^{2-}, NO_3^-, Cl^- and others). For brevity, we represent this composition with the symbol Zn–Al–A. LDHs have gained attention in recent years because of their potential applications in catalysis, drug-delivery, optical devices, bio-sensors and other areas (Cavani *et al* 1991; Choy *et al* 1999; Scavetta *et al* 2007; Costantino *et al* 2008). LDHs intercalated with transition metal complexes are of interest since their decomposition products are mixed-metal oxides and the third metal component improves activity of oxide catalyst (Rives and Ulibarri 1999).

In LDHs, intercalated species is restricted between the close packed metal hydroxide layers which constrains the degrees of freedom of the intercalated species and further limits the growth of solvation sphere. Complex anions ($[ML_n]^{p-}$, M: metal, L: ligand) bond with the hydroxyl groups of the layers and interlayer water through the terminal atom symmetry adapted orbitals (TASOs) of the ligand. TASOs are also involved in bonding with the central metal atom in the transition metal complexes. Hence, one would expect a variation in the electronic structure of the transition metal complex on being confined in the interlayer as opposed to its free state. Transition metal complexes absorb in UV–Vis region of the electromagnetic spectrum due to (i) *d–d* transitions in the metal and (ii) charge transfer (CT) transitions (L→M or M→L). It would be interesting to study the effect of intercalation on these two classes of transitions.

There are several studies on the intercalation of cyano-, halo-, oxo-complexes and complexes containing macrocyclic ligands and the changes in optical, magnetic and other properties brought about by intercalation (Giannelis *et al* 1987; Lopez-Salinas and Ono 1993; Hansen and Koch 1994; Sels *et al* 1999; Venugopal *et al* 2006). The intercalation of the hexacyanoferrates of Fe(II) and Fe(III) into LDH gallery results in a reaction with the metal hydroxide layers leading to the formation of mixed cation hexacyanoferrates, in which some of the cations come from LDH host (Carpani *et al* 2006). Raman studies show that molecular symmetry of the hexacyanoferrates changes to D_{3d} on intercalation within LDH (Frost *et al* 2005). Most of these investigations employ infrared, Mössbauer and X-ray absorption spectroscopies. Fernandez *et al* (1998) report that diffuse reflectance UV–Vis spectra of intercalated hexacyanoferrates are similar to those of the free ion.

In this paper, we focus on changes in the electronic structure of the complex ions resulting from their intercalation between LDH layers. We choose $[Fe(CN)_6]^{4-}$, $[Fe(CN)_6]^{3-}$ (hereafter abbreviated as $[Fe^{II}]$ and $[Fe^{III}]$, respectively) and MnO_4^-, as model systems for the study of *d–d* transition and charge transfer transitions, respectively. We intercalate these model anions in Zn–Al LDH and study their UV–Vis spectra.

2. Experimental

Precursor [Zn–Al–NO_3] LDH was prepared by a co-precipitation technique, wherein 50 mL of a mixed metal nitrate solution ($[Zn^{2+}]/[Al^{3+}] = 2$, total concentration 0·44 M) was added drop wise to a reaction vessel containing 100 mL of $NaNO_3$ salt solution taken 5 times in excess of stoichiometric requirement. A constant pH of 8 was maintained during preparation by adding 0·25 M NaOH solution using Metrohm model 718 STAT Titrino operating in the pH

*Author for correspondence (vishnukamath8@hotmail.com)

STAT mode. N_2 gas was bubbled throughout the preparation and the temperature was maintained at 60 °C. The slurry obtained was aged for 16 h, separated by centrifugation and washed with warm water saturated with N_2.

For the preparation of Zn–Al–A (A = $[Fe(CN)_6]^{3-}$, $[Fe(CN)_6]^{4-}$, $[MnO_4]^-$) LDHs, about 0·5 g of Zn–Al–NO_3, LDH precursor was dispersed in a solution containing potassium salt of the anion (10 times excess of the stoichiometric requirement) which is presaturated with N_2 and stirred for 40 h. The reaction vessel was covered with aluminum foil in order to prevent unwanted photolytic reactions and the precipitate obtained is washed with warm decarbonated water saturated with N_2. The products obtained were dried in a desiccator and stored in the dark to prevent all redox reactions of the intercalated species (Boclair *et al* 2001). The metal contents of the samples were determined by atomic absorption spectroscopy (Varian Model AA240 Atomic Absorption Spectrometer). Samples were digested in acid and total iron content in the case of ferrocyanide/ferricyanide and the total manganese content in the permanganate intercalated sample were determined along with Zn and Al contents. Thermogravimetric studies were carried out using Mettler Toledo 851^e TGA/SDTA system. Samples were dried at 100 °C for 30 min in TG balance to expel adsorbed water and the temperature was ramped from 100–800 °C (5 °C min^{-1}; N_2 atmosphere). The low temperature (T < 200 °C) mass loss yielded intercalated water content of LDHs. From the intercalated anion content and TGA data, approximate formulae of LDHs were determined (table 1). Zn and Al contents in the formulae were adjusted to balance the negative charge due to the estimated content of the intercalated anion. However, this does not match with the actual Zn content estimated by AAS and hence, the formulae given in table 1, are approximate. This divergence was due to Zn dissolution by leaching during anion exchange.

PXRD patterns of all the samples were recorded using Bruker D8 Advance powder diffractometer (source CuKα radiation, λ = 1·5418 Å), at a scan rate of 1° 2θ min^{-1}. IR spectra of the samples were obtained using Shimadzu FTIR-8400S spectrophotometer (KBr pellets, 4 cm^{-1} resolution, 400–4000 cm^{-1}). Diffused reflectance UV–Vis absorption spectra were obtained using Shimadzu ISR-3100 UV–Vis–NIR scanning spectrophotometer. The spectra were recorded from 200–800 nm at a scan rate of 0·83 nm s^{-1}. Where overlapping bands are observed, these are deconvoluted into Gaussian components using Peakfit (2007) version 4·12 software (Peakfit SeaSolve Software). UV–Vis spectrum of the precursor Zn–Al–NO_3 LDH was recorded to ensure that there was no absorption due to the host LDH in the region, where the absorptions due to the anions ($[Fe(CN)_6]^{3-}$, $[Fe(CN)_6]^{4-}$, $[MnO_4]^-$) are expected. So the observed spectra were solely due to the intercalated species.

3. Results and discussion

3.1 *Ferricyanide, ferrocyanide intercalated LDHs*

PXRD patterns obtained for Zn–Al–[Fe^{II}] and Zn–Al–[Fe^{III}] LDHs are shown along with that of Zn–Al–NO_3 LDH in figure 1. Increase in the basal spacing from 8·8 Å in NO_3^-–LDH to 11 Å in the case of ferricyanide–LDH and 10·89 Å in the case of ferrocyanide–LDH upon exchange, confirms the intercalation of these species into LDH gallery. XRD peaks obtained in the case of ferricyanide intercalated LDH could be indexed to a phase with rhombohedral symmetry (a = 3·075 Å and c = 32·9 Å). Further, IR spectra (figure 2) confirm intercalation of the ions into LDH. Zn–Al–[Fe^{III}] LDH shows a band at 2112 cm^{-1} characteristic of C≡N stretch with Fe in +3 oxidation state, whereas Zn–Al–[Fe^{II}] LDH shows a band at 2025 cm^{-1}. The frequency of C≡N stretch is highly sensitive to oxidation state of the iron in the complex (Tosi and Danon 1964). Absence of the band at 2040 cm^{-1} in the spectrum of Zn–Al–[Fe^{III}] LDH suggests that there is no reduction of Fe(III) to Fe(II) as reported earlier (Idemura *et al* 1989; Fernandez *et al* 1998). Similarly, absence of band in the region of 2110 cm^{-1} in the case of Zn–Al–[Fe^{II}] LDH indicates that there is no oxidation of Fe(II) to Fe(III).

The composition of the precursor and anion-exchanged LDHs are given in table 1. Zn/Al ratio in the precursor LDHs is close to 2 and upon exchange with the complexes there is a decrease in the ratio, which may be attributed to dissolution of LDH during exchange. Al/Fe ratios show that in both Zn–Al–[Fe^{III}] and Zn–Al–[Fe^{II}] LDHs the iron content is less than the stoichiometric requirement. This suggests the presence of residual nitrate in the exchanged samples which is evident in IR spectra.

TGA data overlaid with DTG curve for Zn–Al–[Fe^{III}] and Zn–Al–[Fe^{II}] LDHs are shown in figure 3. The mass loss observed below 200 °C is attributed to the removal of intercalated water. The water content present in the sample is found to be 0·68 moles per formula unit in the case of Zn–Al–[Fe^{III}]

Table 1. Results of wet-chemical analysis and TGA of LDHs used.

LDH	Zn/Al	Al/Fe (Mn)	Water content	Approximate formula
Zn–Al–NO_3	2·1	–	0·72	$Zn_{0·67}Al_{0·32}(OH)_2 \cdot 0·72H_2O$
Zn–Al–[Fe^{III}]	2·06	3·4(3·0)*	0·68	$Zn_{0·67}Al_{0·32}(OH)_2[Fe(CN)_6]_{0·094} \cdot 0·68H_2O$
Zn–Al–[Fe^{II}]	1·7	4·5(4·0)	0·64	$Zn_{0·60}Al_{0·32}(OH)_2[Fe(CN)_6]_{0·071} \cdot 0·64H_2O$
Zn–Al–MnO_4	1·8	0·9(1·0)	0·54	$Zn_{0·60}Al_{0·32}(OH)_2[MnO_4]_{0·03} \cdot 0·54H_2O$

*Numbers given in parentheses are expected values.

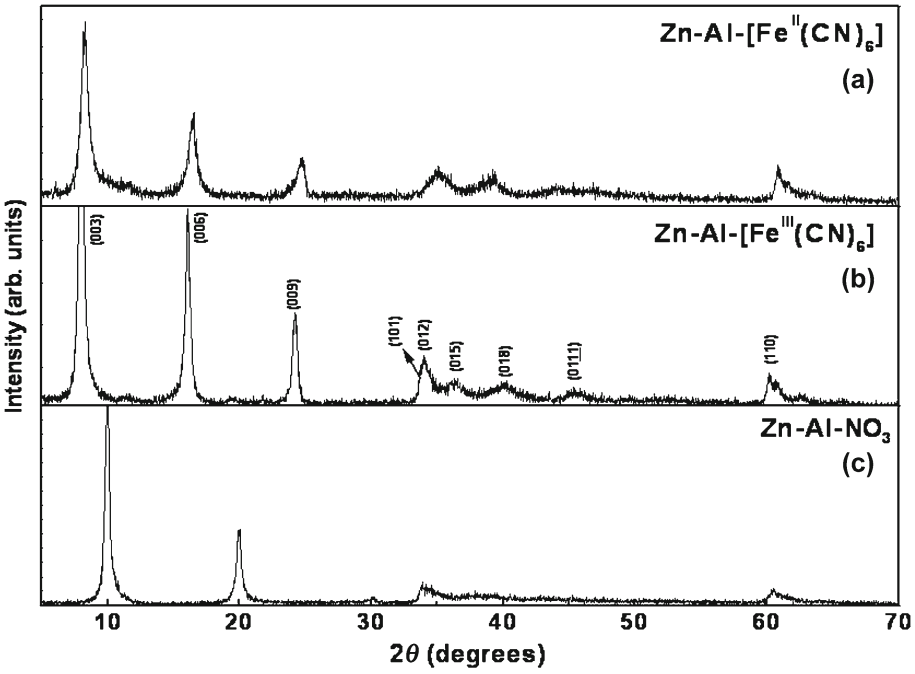

Figure 1. PXRD patterns of (a) Zn–Al–NO_3, (b) Zn–Al–[$Fe^{III}(CN)_6$] and (c) Zn–Al–[$Fe^{II}(CN)_6$] LDHs.

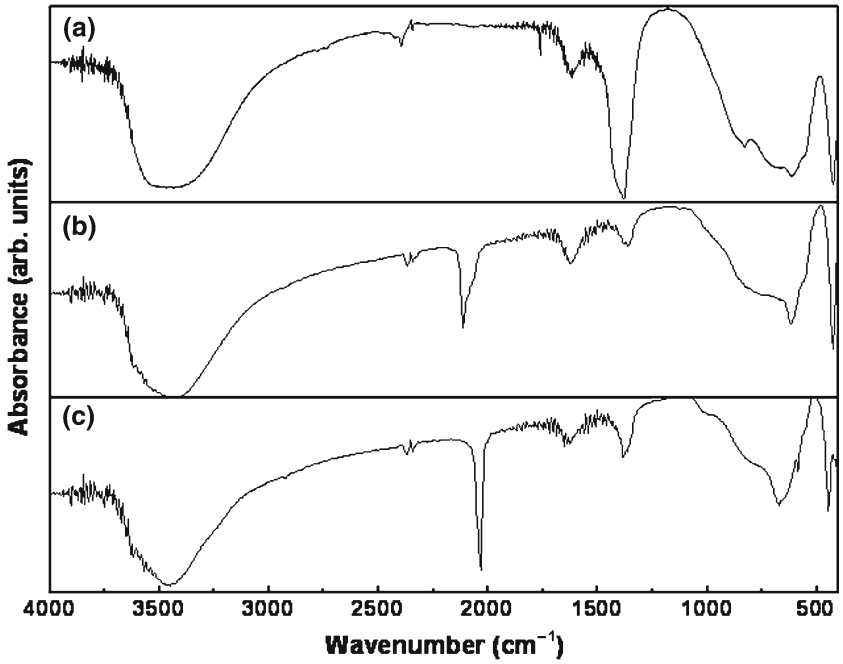

Figure 2. IR spectra of (**a**) Zn–Al–NO_3, (**b**) Zn–Al–[$Fe^{III}(CN)_6$] and (**c**) Zn–Al–[$Fe^{II}(CN)_6$] LDHs.

and 0·64 moles per formula unit in the case of Zn–Al–[Fe^{II}] LDH.

A comparison of UV–Vis spectrum of Zn–Al–[Fe^{III}] LDH with that of pure salt (figure 4) shows that all the bands are shifted to a lower energy and the extent of shift of each band is listed in table 2. The bands observed for $K_3[Fe(CN)_6]$ are assigned according to Alexander and Gray (1968). In $[Fe(CN)_6]^{3-}$, iron is in d^5 configuration with a hole in t_{2g} level, which permits ligand to metal charge transfer (LMCT), which are intense transitions, along with weak *d*–*d* bands. LMCT to metal t_{2g} level are observed in UV–Vis region, whereas LMCT transitions to the metal e_g level lie in the

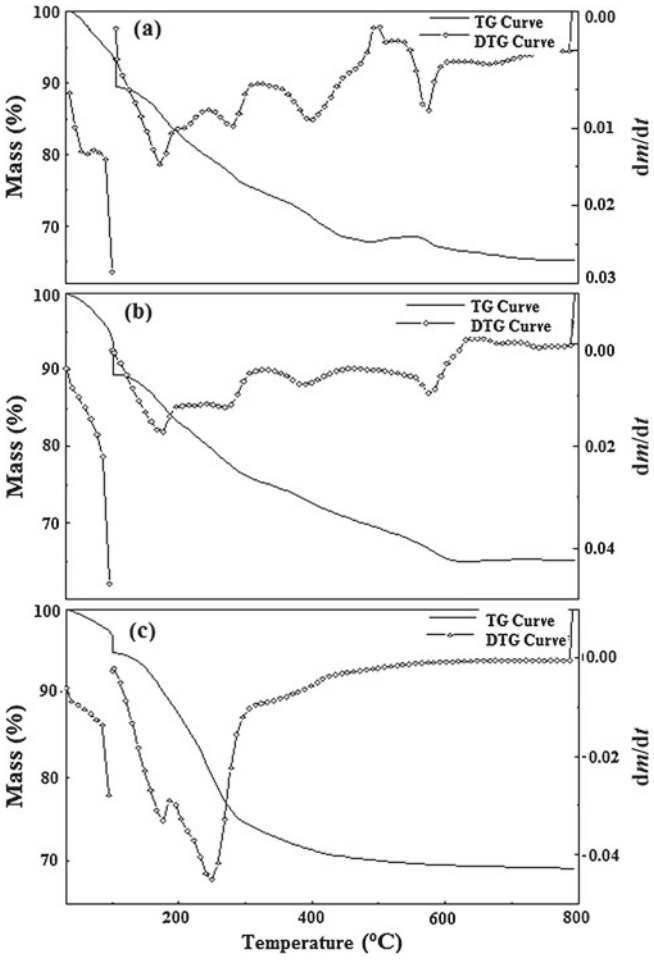

Figure 3. TG–DTG curves of (**a**) Zn–Al–$[Fe^{III}(CN)_6]$, (**b**) Zn–Al–$[Fe^{II}(CN)_6]$ LDHs and (**c**) Zn–Al–MnO_4 LDH. The mass loss at 100 °C is due to *in situ* drying (100 °C, 30 min stay).

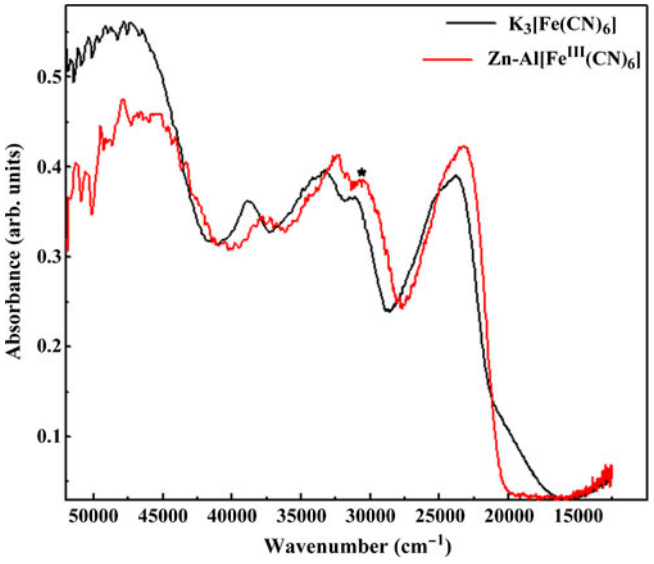

Figure 4. UV–Visible spectra of Zn–Al–$[Fe^{III}(CN)_6]$ LDH overlaid with that of $K_3[Fe(CN)_6]$. Feature marked with an asterisk is due to *d–d* transition.

vacuum UV region. The bands at 38,700, 33,250, 23,740 cm^{-1} in $K_3[Fe(CN)_6]$ are assigned to LMCT from low lying ligand orbitals to metal t_{2g}. These transitions in LDH shift to red and are observed at 37,650, 32,325 and 23,170 cm^{-1}. The weak band corresponding to 31,200 cm^{-1} (30,366 cm^{-1} on intercalation) is assigned to *d–d* transition.

Similar data of Zn–Al–$[Fe^{II}]$ LDH show that the absorptions due to intercalated $[Fe(CN)_6]^{4-}$ ion are shifted to higher wavenumbers compared to pure salt (figure 5). The bands observed are assigned according to Gray and Beach (1963). In $[Fe(CN)_6]^{4-}$, iron is in d^6 configuration and since, CN^- is a strong field ligand, it forms low spin complex with t_{2g} level completely filled to give $^1A_{1g}$ ground state with the configuration $(3t_{1u})^6(2t_{2g})^6$. All LMCT transition from low lying ligand orbitals must terminate on the high energy e_g level and these would appear in the vacuum UV region. On the other hand, metal to ligand charge transfer (MLCT) transitions from t_{2g} to anti-bonding ligand orbitals are expected and they are commonly observed (Lever 1985). The overlapping bands observed in $K_4[Fe(CN)_6]$ and Zn–Al–$[Fe^{II}]$ LDH are decomposed into Gaussian components and the absorption maxima and FWHM values of the constituent Gaussian bands are listed in table 3. The absorption observed at 29,761 cm^{-1} in $K_4[Fe(CN)_6]$ is assigned to *d–d* transition from $2t_{2g} \rightarrow 3e_g$, which in the case of LDH shifts towards blue and is observed at 30,950 cm^{-1}. The band observed at 44,050 cm^{-1} in $K_4[Fe(CN)_6]$ is assigned to one of the CT transitions from metal to ligand which does not show much shift on intercalation. The weak band observed at ~36,000 cm^{-1} is assigned to be the other *d–d* transition which in the LDH sample is masked by the strong CT band and on peak, decomposition is observed at 38,314 cm^{-1}.

3.2 *MnO_4^- containing LDH*

PXRD pattern and the corresponding IR spectrum of Zn–Al–MnO_4^- LDH are shown in figure 6. The diminished NO_3^- peak at 1380 cm^{-1} in IR spectrum and the appearance of a peak at 910 cm^{-1} indicates that MnO_4^- is intercalated in the interlayer (Villegas *et al* 2003). TG data obtained for LDH overlaid with DTG curve (figure 3) indicates three mass loss steps. The mass loss below 200 °C is attributed to the removal of adsorbed and intercalated water. The amount of water present in the interlayer of LDH is found to be 0·54 moles per unit formula (table 1). UV–Vis spectrum of MnO_4^- LDH is compared with that of $KMnO_4$ (figure 7). The overlapping bands in the spectra are decomposed into their Gaussian components. The bands observed for $KMnO_4$ are assigned according to Viste and Gray (1964). In MnO_4^-, Mn is in d^0 configuration and all the bands observed are due to L→M charge transfer transitions. Three prominent bands are seen in UV–Vis spectrum of $KMnO_4$ and are observed at 31,347, 18,939 and 14,662 cm^{-1}. The intense band observed at 31,347 cm^{-1} is assigned to $3t_2 \rightarrow 2e$ transition, whereas the band observed at 18,939 cm^{-1} is assigned to $t_1 \rightarrow 2e$ transition and the band at 14,662 cm^{-1} to the spin-forbidden

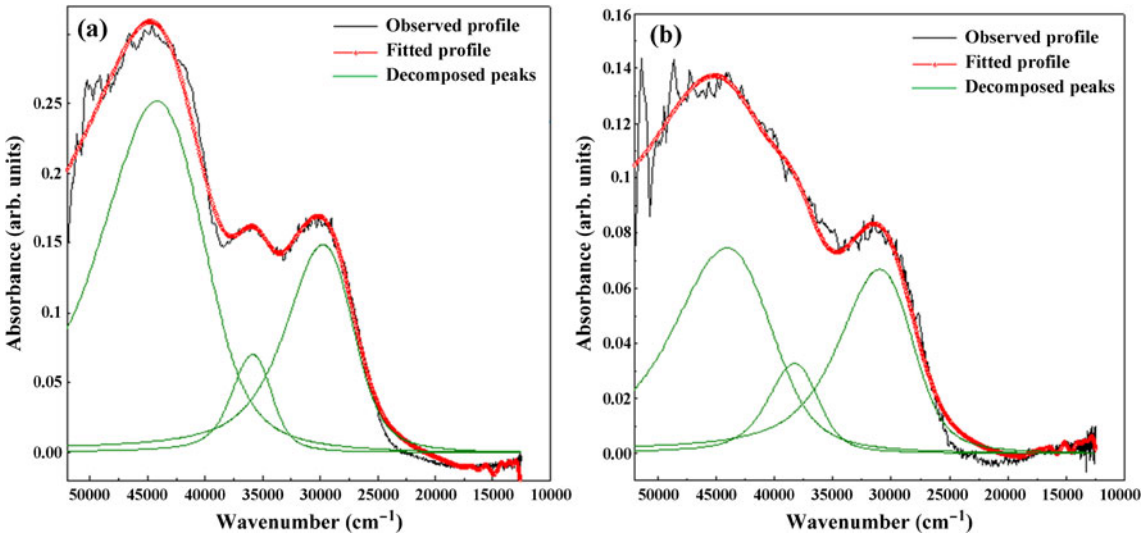

Figure 5. UV–Visible spectra of (**a**) $K_4[Fe(CN)_6]$ and (**b**) Zn–Al–$[Fe^{II}(CN)_6]$ LDHs with their decomposed Gaussian components.

Table 2. List of band positions observed for potassium salts of anion and LDH samples.

Salts	Peak position (cm^{-1})	LDH	Peak position (cm^{-1})
$K_3[Fe(CN)_6]$	38,700	Zn–Al–$Fe^{III}(CN)_6$	37,650
	33,250		32,325
	31,200 (*d*–*d*)		30,366
	23,740		23,170
$K_4[Fe(CN)_6]$	44,050	Zn–Al–$Fe^{II}(CN)_6$	44,052
	35,842 (*d*–*d*)		38,314
	29,761 (*d*–*d*)		30,950
$KMnO_4$	31,347	Zn–Al–MnO_4	31,387
	18,939		23,758
	14,662		18,695

Table 3. List of band centres and FWHM values obtained after decomposition of the observed UV–Vis spectra.

Samples	Peak centre (nm)	FWHM values (nm)
$K_4[Fe(CN)_6]$	227·0	65·3
	279·1	65·3
	336·2	65·3
Zn–Al–$Fe(CN)_6$	227·7	71·6
	261·8	71·6
	323·1	71·6
$KMnO_4$	319·0	169·6
	528·6	169·6
	682·5	169·6
Zn–Al–MnO_4	318·6	125·1
	420·9	125·1
	534·9	125·1

$t_1 \rightarrow 2e$ transition. In MnO_4^-–LDH, a single broad asymmetric band is observed indicating the overlapping of bands which upon decomposition into Gaussian components yields absorptions at 31,387, 23,758 and 18,695 cm^{-1}. While the latter two bands are blue shifted compared to $KMnO_4$ bands, the first band at 31,387 cm^{-1} remains almost at the same position.

The interaction between the metal hydroxide layer and the interlayer species in layered double hydroxides is governed mainly by two kinds of interactions: (i) electrostatic interactions and (ii) hydrogen bonding with the layer hydroxyl groups and with water molecules of the interlayer, which get incorporated into interlayer during the course of preparation. These interactions substantially affect the electronic structure of the intercalated ions by perturbation of TASOs.

In the case of $[Fe(CN)_6]^{3-}$ and $[Fe(CN)_6]^{4-}$, the CN^- group is coordinated to Fe through C and N is the free

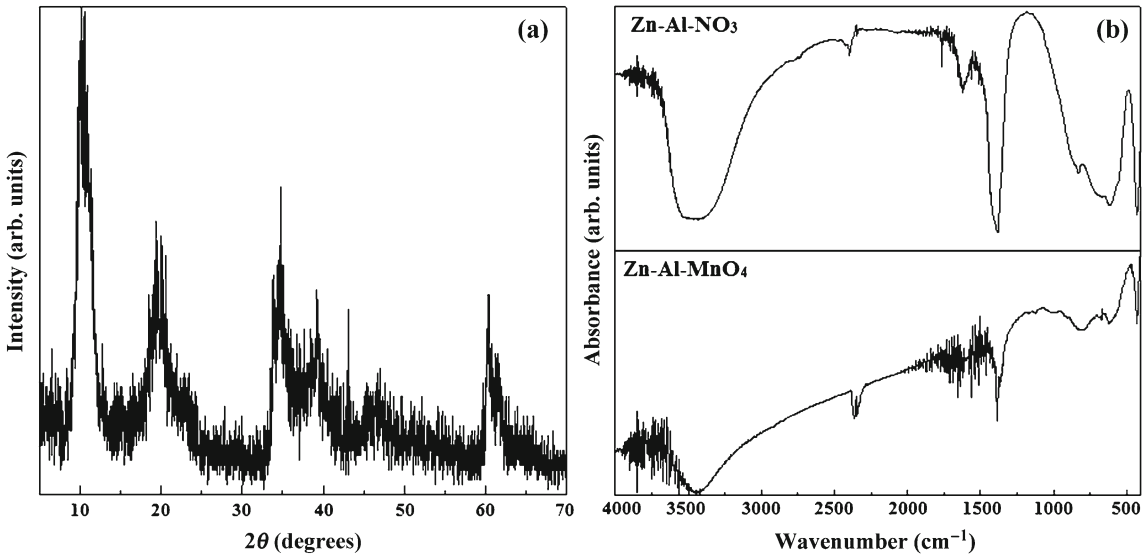

Figure 6. (**a**) PXRD pattern of Zn–Al–MnO_4 LDH, (**b**) IR spectra of Zn–Al–NO_3 and Zn–Al–MnO_4 LDHs.

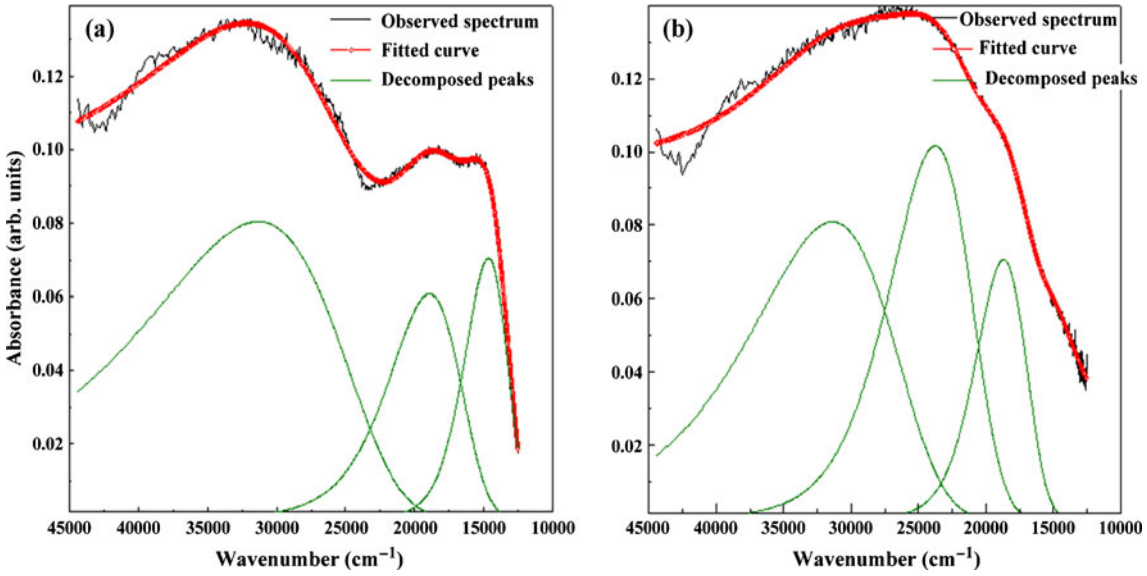

Figure 7. UV–Visible spectra of (**a**) $KMnO_4$ and (**b**) Zn–Al–MnO_4 LDH with their decomposed Gaussian components.

end. CN^- is a strong σ-donor and a weak π-acceptor ligand. Upon intercalation into LDH gallery, the free end of the ligand, CN^- is involved in hydrogen bonding with the layer hydroxyls and the water molecules of the interlayer. This causes a decrease in electron density on the ligand group orbitals, TASOs and hence, reduces σ-donor character of the ligand while increasing its π-acceptor character (Shriver and Posner 1966). This increases the ligand field strength and hence, the separation between e_g and t_{2g} levels. So all LMCT transitions to t_{2g} levels are expected to experience a red shift, while transitions to e_g level are expected to be blue shifted. Further, the *d–d* and MLCT transitions arising from t_{2g} level are expected to be blue shifted.

In ferricyanide ion, as mentioned earlier, the *d–d* transitions are weak and are further obscured by intense CT bands arising from low lying ligand orbitals to metal t_{2g} level. On intercalation into LDH, LMCT bands are observed to undergo a red shift as expected.

In case of the ferrocyanide ion, two *d–d* transitions and one MLCT transition are observed. The two *d–d* transition bands are shifted to blue in LDH compared to $K_4Fe(CN)_6$ as expected. The other band observed at 44,052 cm^{-1} is M→L CT transition and does not show much shift in its position in LDH sample and the reason is not clear.

In MnO_4^-, all the transitions are from non-bonding $p\pi$ orbital (t_1) of oxygen and $3t_2$ level of oxygen to σ-antibonding orbital of Mn. Upon intercalation into LDH gallery, the non-bonding $p\pi$ electrons are involved in hydrogen bonding with hydroxyl groups of the metal hydroxide layer and water molecules present in the interlayer, which

stabilizes the energy of t_1 level. This being the case one expects a blue shift in the transition arising from this level. In the case of LDH sample, a single broad, asymmetric band is observed. Two CT bands of LDH (23,758 and 18,695 cm^{-1}) are from non-bonding $p\pi$ orbital of oxygen to σ-antibonding level of Mn and are indeed blue shifted. The other band at 31,387 cm^{-1} is due to transition from $3t_2$ of oxygen to σ-antibonding orbital of Mn. Since, $3t_2$ orbital of MnO_4^- is less involved in any of the interactions with the interlayer, this band remains invariant.

Apart from the factors discussed above, there are several other factors that influence the observed UV–Vis spectra of LDH samples, which are highly complicated to predict. Further, the extent of shift observed is not explained since it requires the quantification of various interactions involved.

4. Conclusions

We report here transition metal complex intercalated LDHs and study the effect of intercalation on their UV–Vis bands for which, we have chosen ferrocyanide/ferrocyanide and permanganate ions as candidate anions for *d–d* and CT transitions, respectively. Shift in the position of UV–Vis bands is observed in all the cases. We interpret the shift in bands based on the variation in ligand field strength of the metal complex upon intercalation into LDH interlayer due to various interactions involved with the host.

Acknowledgements

The authors thank Prof E Arunan for useful discussions and the Department of Science and Technology (DST), Government of India (GOI), for financial support. (S R) is grateful to the Council for Scientific and Industrial Research, GOI, for the award of a senior research fellowship. (PVK) is a recipient of the Ramanna fellowship of DST.

References

Alexander J J and Gray H B 1968 *J. Am. Chem. Soc.* **90** 4260

Boclair J W, Braterman P S, Brister B D, Wang Z and Yarberry F 2001 *J. Solid State Chem.* **161** 249

Carpani I, Berrettoni M, Giorgetti M and Tonelli D 2006 *J. Phys. Chem.* **B110** 7265

Cavani F, Trifiro F and Vaccari A 1991 *Catal. Today* **11** 173

Choy J H, Kwak S Y, Park J S, Jeong Y J and Portier J 1999 *J. Am. Chem. Soc.* **121** 1399

Costantino U, Ambrogi V, Nocchetti M and Perioli L 2008 *Micropor. Mesopor. Mater.* **107** 149

Fernandez J M, Ulibarri M A, Labajos F M and Rives V 1998 *J. Mater. Chem.* **8** 2507

Frost R L, Musumeci A W, Bouzaid J, Adebajo M O, Martens W N and Kloprogge J T 2005 *J. Solid State Chem.* **178** 1940

Giannelis E P, Nocera D G and Pinnavaia T J 1987 *Inorg. Chem.* **26** 203

Gray H B and Beach N A 1963 *J. Am. Chem. Soc.* **85** 2922

Hansen H C B and Koch C B 1994 *Clays Clay Miner.* **42** 170

Idemura S, Suzuki E and Ono Y 1989 *Clays Clay Miner.* **37** 553

Lever A B P 1985 *Inorganic electronic spectroscopy* (ed.) M F Lappert (London: Elsevier)

Lopez-Salinas E and Ono Y 1993 *Micropor. Mater.* **1** 33

Miyata S 1975 *Clays Clay Miner.* **23** 369

Peakfit Software (2007) Version 4.12 SeaSolve Software Inc., 235 Walnut St., Suite Framingham, MA 01702

Rives V and Ulibarri M A 1999 *Coord. Chem. Rev.* **181** 61

Scavetta E, Scavetta S, Stipa S, Stipa D and Tonelli D 2007 *Electrochem. Commun.* **9** 2838

Sels B F, De Vos D E, Grobet J P, Pierard F, Mesmaeker F K D and Jacobs P A 1999 *J. Phys. Chem.* **B103** 1111

Shriver D F and Posner J 1966 *J. Am. Chem. Soc.* **88** 1672

Tosi L and Danon J 1964 *Inorg. Chem.* **3** 150

Venugopal B R, Ravishankar N, Christopher Perrey R, Shivakumara C and Michael Rajamathi 2006 *J. Phys. Chem.* **B110** 772

Villegas J C, Giraldo O H, Laubernds K and Suib S L 2003 *Inorg. Chem.* **42** 5621

Viste A and Gray H B 1964 *J. Am. Chem. Soc.* **86** 1113